ACTION CURRENTS, INTERNODAL POTENTIALS, AND EXTRACELLULAR RECORDS OF MYELINATED MAMMALIAN NERVE FIBERS DERIVED FROM NODE POTENTIALS

WILLIAM B. MARKS *and* GERALD E. LOEB

From the Laboratory of Neural Control, National Institute of Neurological and Communicative Disorders and Stroke, National Institutes of Health, Bethesda, Maryland 20014

ABSTRACT The potential distribution within the internodal axon of mammalian nerve fibers is derived by applying known node potential waveforms to the ends of an equivalent circuit model of the internode. The complete spatial/temporal profile of action potentials synthesized from the internodal profiles is used to compute the node current waveform, and the extracellular action potential around fibers captured within a tubular electrode. For amphibia, the results agreed with empirical values. For mammals, the amplitude of the node currents plotted against conduction velocity was fitted by a straight line. The extracellular potential waveform depended on the location of the nodes within the tube. For tubes of length from 2 to 8 internodes, extracellular wave amplitude (mammals) was about one-third of the product of peak node current and tube resistance (center to ends). The extracellular potentials developed by longitudinal and radial currents in an anisotropic medium (fiber bundle) are compared.

INTRODUCTION

Single unit recordings from nerve fibers are often made by dissecting small bundles free from the surrounding tissue and placing them in contact with a macroelectrode (e.g. a wire hook) in a confining insulating medium (e.g., air, mineral oil, plastic sleeves). This facilitates the recording by stabilizing the spatial relationship of nerve fiber and electrode, amplifying the action potential by forcing the current through a high extracellular resistance, and permitting a metal contact of large surface area and low junction impedance and thermal noise. Several investigators are developing this configuration to record chronically from multiple fibers confined to solid insulating tube electrodes either by dissection and insertion (Brindley, 1972; Hoffer et al., 1974) or by regeneration of cut tracts (Mannard et al., 1974; see also Marks, 1965).

An understanding of the influence of the size of the fibers and of the fiber bundle, and of the tube length and diameter, on the amplitude and waveform of the recorded potentials is needed to guide experiments and the design of electrodes. Stein and Pearson (1971) have calculated the potentials to be expected from invertebrate unmye-

linated fibers in tubes, and they have also derived a simple proportional relationship between the extracellular potential within a tube and the spatial profile of the intra-axonal potential of unmyelinated fibers. This relationship applies to myelinated fibers as well (see below). Thus we require the spatial profile of the intra-axonal potential of myelinated fibers. For amphibian fibers, this has been measured by Huxley and Stampfli (1949) and derived from voltage clamp data by Fitzhugh (1962) and Goldman and Albus (1968). Such data are not available for mammalian fibers.

This paper presents an alternate method for calculating the spatial profile of the internodal intra-axonal potential from the time course of the action potential at a node, which has been determined for a large range of mammalian myelinated fiber sizes (Paintal, 1966, 1967). This spatial/temporal profile of the action potentials is then used to predict the node currents (for myelinated mammalian fibers having conduction velocities from 8 to 100 m/s), and the amplitudes and waveforms of action potentials which would be recorded from these fibers in tubes of varying length and position with respect to the nodes. The validity of this method is discussed by comparing the theoretical with experimentally determined action currents for mammalian and amphibian myelinated fibers.

The following list of symbols gives the variables used, and the constants together with their sources.

LIST OF SYMBOLS

Variables

C	Conduction velocity
C_m	Myelin capacitance per unit length
D	Tube diameter
d	Axon diameter = myelin i.d.
d'	Fiber diameter = myelin o.d.
$E(t)$	Empirical intra-axonal potential at node
i	Myelin or membrane current per unit length
i_{node}	Node current
I_e	Longitudinal current outside fiber
I_i	Longitudinal current within fiber
J_x	Longitudinal current density outside fiber
L	Internode length
L'	Tube length
r	Radial coordinate within tube electrode
r_m	Myelin resistance times unit length
R_e	Extracellular resistance per unit length within tube
R_i	Intra-axonal resistance per unit length within tube
R_t	Tube resistance, center to ends
r^*	Radial distance from node
s_x	Longitudinal extracellular conductivity
t	Time
T_d	Duration of action potential
T_r	Rise time of action potential
$u(r^*, x)$	Potential distribution about node

$V(t, x)$ Intra-axonal potential
$V_0(t, x)$ Intra-axonal potential along 0th internode
$v(x)$ Average of $w(r, \theta, x)$ over cross section of tube
$w(r, \theta, x)$ Extracellular potential distribution about axis of tube
x Distance along axon

Constants

K_0 Capacitivity of vacuum = $8.85\,(10)^{-10}$ F/cm
K_m Dielectric constant of myelin = 5–10 (Hodgkin, 1964, p. 53)
K_2 Specific resistivity of myelin = $5\text{–}8\,(10)^{14}$ Ω-cm (Hodgkin, 1964)
K_i Axoplasmic resistivity = 110 Ω-cm for frog (Stampfli, 1952), = 110(65/80) = 90 Ω-cm for cat
K_x Longitudinal resistivity of nerve trunk = 2.5(65 Ω-cm) = 163 Ω-cm (Tasaki, 1964, corrected for mammalian saline)
K_t Transverse resistivity of nerve trunk = 120(65 Ω-cm) = 7800 Ω-cm (Tasaki, 1964)

INTRA-AXONAL POTENTIALS

Theory

With Fitzhugh (1962), we model the internode as a linear distributed leaky cable: an intra-axonal resistance per unit length R_i shunted by the distributed myelin capacitance C_m and resistance r_m to the external medium, which we place at ground potential, ignoring the extracellular potential drops for the present. The resistance of the parallel extracellular paths is less than 0.02 times that of the intracellular paths, even though they are constricted by the anisotropy of the extracellular medium (see below). Clark and Plonsey (1966, 1968) have shown that transverse voltage differences within axons can be ignored for most purposes, so that the intra-axonal potential can be represented along a single length coordinate. The intra-axonal potential $V(t, x)$ then obeys the following equation in the internode (i is myelin current per unit length):

$$i = C_m \delta V/\delta t + V/r_m = (1/R_i)\,\delta^2 V/\delta x^2. \tag{1}$$

The boundary conditions at the nodes $x = 0, L$ are

$$V(t, 0) = E(t), \qquad V(t, L) = E(t - L/C), \tag{2}$$

where $E(t)$ is the empirical node potential. The resting potential was ignored.

Eq. 1 was converted into a difference equation and solved by iterative relaxation from the initial condition $V(t, x) = (1 - x/L)\,V(t, 0) + (x/L)\,V(t, L)$ as follows. In each iteration the new value of V at each point on the (t, x) plane was calculated using Eq. 1 from the old values at the four adjacent grid points. Initially $dx = L/5$. When each series of iterations converged (i.e., did not change, so that Eq. 1 was satisfied), dx was reduced by $\frac{1}{2}$, and a new series of iterations made until $dx < 25$ μm. Throughout, dt = wave duration/(number of samples); there were 72 samples for cat, 80 for frog. The resulting internodal potential was taken as that for internode 0, $V_0(t, x)$, valid for $0 < x < L$. For t outside the duration of the wave, $0 < t < T_d$, $V_0(t, x) = 0$. The value of $V(t, x)$ for x perhaps outside the calculated interval, but within the kth

internode, was computed from

$$V(t, x) = V_0(t + kL/C, x - kL), \quad (3)$$

where $0 < x - kL < L$, k an integer. Expressed as a difference equation in which t and x occurred only at sample points, this relation required (third order) interpolation between the calculated sample points, since the required positions and times in Eq. 3 fell between those calculated for internode 0. Thus we obtained the value of $V(t, x)$ for a range of x and t equal to the entire duration, T_d, and wavelength $0 < x < C\ T_d$, of the action potential. The (inward) node current was calculated from

$$i_{node} = \lim (e \to 0)(1/R_i)[\delta V/\delta x(x = e) - \delta V/\delta x(x = -e)]. \quad (4)$$

Node Potentials

Paintal (1966; 1967) dissected the vagus and saphenous nerves of the cat, and recorded monophasic unit potentials under oil on hooks. The amplifier frequency range was 0.06 Hz to 37 kHz. One hook was in contact with the cut end of the fiber, and the other one was 1 mm distant from the end. The latter hook was a ground for the outside of the fiber, while the hook on the cut end was resistively connected to ground and, through the inside of the fiber, to the first node, 0–2 mm away. It therefore recorded an attenuated copy of the node potential, except for capacitatively coupled myelin currents which flowed in the intra-axonal resistance, and except for the possibility of damage to the first node. The capacitance, and damage probably also, would tend to make the recorded waveform slower than the waveform of a normal node. However, these records are not slower than intra-axonal potentials recorded by Eccles and

TABLE I

FIBER PARAMETERS AND ACTION CURRENTS

C	d'	d	d'/d	L	T_r	T_d/T_r	i_{node}		
m/s	*μm*	*μm*		*μm*	*μs*		*nA*		
Frog									
23	14.0	10.0	0.72	2,000	0.18	5.7	4.09		
Cat									
8	2.1	0.6	0.29	200	0.20	5.0	0.13		
16	3.3	1.4	0.43	313	0.13	3.7	0.44		
64	11.5	6.9	0.60	1,092	0.10	3.6	3.31	2.37*C* 3.67*E*	3.17*R* 0.77*L*
80	14.2	8.5	0.60	1,344	0.09	3.7	4.44		
100	17.4	10.3	0.59	1,634	0.08	3.9	5.88		

The fiber (d') and axon (d) diameters are from Sanders and Whitteridge (1946) and Williams and Wendell-Smith (1971), the internodal lengths from Lubinska (1960), and the rise times (T_r) and spike durations (T_d) from Paintal (1966) for cat, and Goldman and Albus (1968) for frog. For the 64 m/s fiber, computed node currents for four modified conditions are added: for the dielectric constant K_m set to 6 instead of 10 (C); for the myelin resistivity K_2 increased 10 times (R); for an accelerated node potential waveform (E) (see Fig. 1), and for L = 200 μm (anticipated internode after regeneration) (L). These currents also appear in Fig. 4.

Krnjevic (1959) from dorsal root fibers after their entrance into the spinal cord of cats. Measuring times from these records in the manner of Paintal, i.e. extrapolating from the point of fastest slope to the base line, one finds a rise-time of about 0.1 ms, and a duration of 0.4 ms. The data of Paintal (1966) yield 0.08 ms for the rise-time and 0.31 ms for the duration of action potentials conducted at the same velocity (100 m/s, extrapolating from his maximum value of 80 m/s; see Table I).

Although Paintal measured many rise and fall times, he only published a few waveforms, and these all resembled that for his 64 m/s fibers. Since the ratio of rise-time to duration of all the spikes with velocity between 8 and 100 m/s were approximately constant (see Table I), we have adopted the 64 m/s waveform for all velocities, except to scale them to fit the data for rise-time.

The amplitudes of the action potential waveforms from cat were adjusted to 130 mV. This estimate of the intracellular amplitude was obtained by Horakova et al. (1968) from single nodes of rat sciatic nerve fibers using an air gap and current clamp. The resulting node potential waveform labeled "cat" is shown in Fig. 1 for two conduction velocities. The dashed waveform in Fig. 1 was obtained by adding to the node potential for cat its own time derivative multiplied by 16.6 μs. This "accelerated" wave was used to check the effect on our results of a possible capacitative slowing of the empirical node potential.

The action potential in Fig. 1 labeled "frog" was recorded by Hodler et al. (1952), also from a cut end. This curve, too, may be slower than the underlying node potential. Its rise-time (0.20 vs. 0.15 ms) and duration (1.1 vs. 1.2 ms), are similar to the propagated action potentials of *Xenopus* computed by Goldman and Albus (1968) from voltage clamp data, but its foot and peak are more rounded. Its amplitude was scaled to 115 mV (Huxley and Stampfli, 1949; Frankenhaeuser and Huxley, 1964).

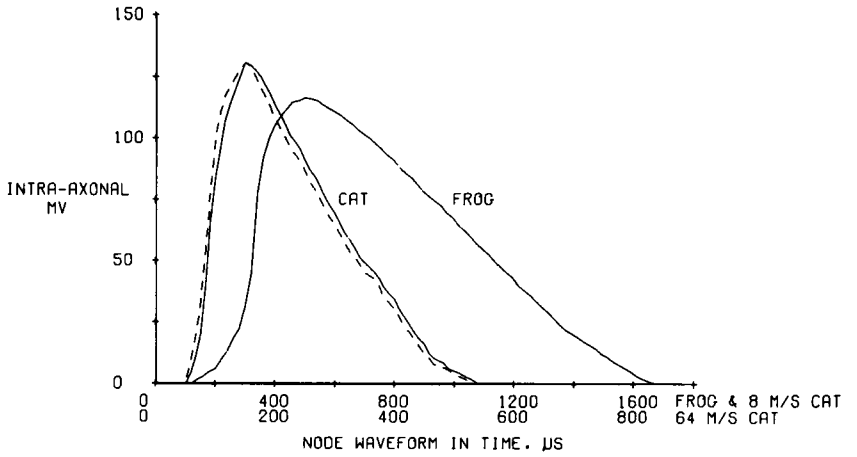

FIGURE 1 Empirical waveforms which were used as node potentials. The dashed curve is the waveform for cat augmented by its time derivative times 16.6 μs.

The Properties of the Internode

Among the other quantities required for computation, the internodal length, myelin thickness, and fiber diameter are known for the full range of mammalian fibers. However, the internodal myelin capacity and resistance, and the internal longitudinal resistance of the axon had to be adapted from those of amphibia.

Those properties which vary with conduction velocity (C), namely axon diameter (d), fiber diameter (d'), length of internode (L), waveform rise-time (T_r), and duration/T_r, appear in Table 1 with associated sources. Note that d/d' is not constant, but drops below 0.60 for $C < 16$ m/s. The myelin capacitance per unit length was computed from the relation

$$C_m = 2\pi K_0 K_m / \ln (d'/d). \tag{5}$$

(Eqs. 5, 6, and 7 can be found in physics texts.) The values and sources of the constants are given in the list of symbols. K_m, the dielectric constant of myelin, was assumed to be that of amphibia, 6–10. The effect of reducing it from 10 to 6 was investigated, and the amplitude of the resulting node current appears in line 4 of Table I. The transmyelin resistance times unit length was given by

$$r_m = (K_2/2\pi) \ln (d'/d), \tag{6}$$

where the specific resistance of myelin, K_2, was assumed to be the same as for amphibia. The effect of uncertainties in K_2 was gauged by recalculating the amplitude of the node current for K_2 increased by a factor of 10. This appears in Table I, line 4. The axoplasmic resistance per unit length was given by

$$R_i = K_i/\pi (d/2)^2. \tag{7}$$

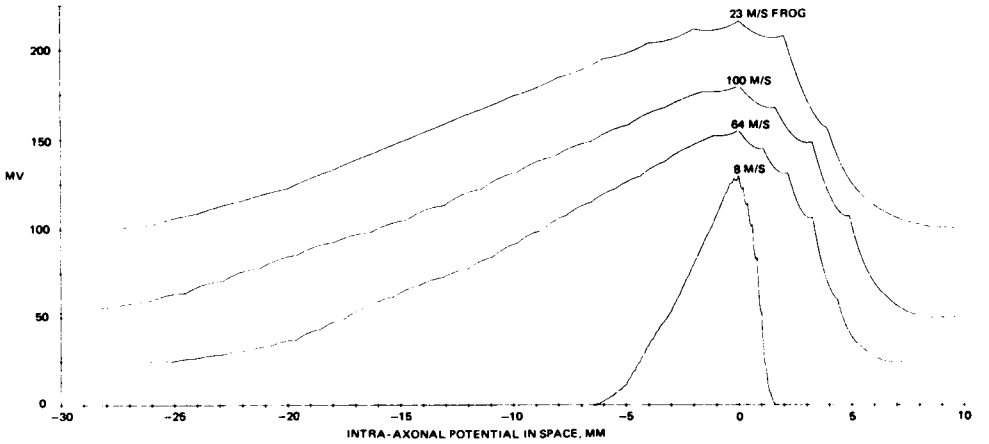

FIGURE 2 Spatial profiles of intra-axonal potential at the moment when the node potential at $x = 0$ is maximum, for fibers of several sizes, calculated from the node potentials by solving Eq. 1.

Derived Intra-axonal Voltage Profile

$V(t, x)$ was calculated for the nine varieties of cat nerve fiber and one of the frog listed in Table I. Some of these profiles are illustrated in Fig. 2 for waves propagating to the right at the moment when the node at $x = 0$ is at maximum depolarization. The dips in the amphibian internodes resemble those measured by Huxley and Stampfli (1949) and calculated by Fitzhugh (1962) and by Goldman and Albus (1968), all for the same large amphibian sciatic nerve fibers to which our curve applies. For each, the maximum amplitude of the dips was about 5.0 mV, except for the curves of Goldman and Albus (1968), who assumed a shorter internode and found 3.3 mV.

Derived Node and Myelin Currents

Fig. 3 shows node current waveforms calculated from the gradients of the potential profiles of Fig. 2 immediately adjacent to a node (Eq. 4). Inward currents are plotted upwards. The solid curve labeled "23 m/s frog" is our frog node current, and the curve in small dots, scaled to the same height for comparison, is the average of several measurements of node current from a frog nerve by Huxley and Stampfli (1949). The actual amplitude of the inward phase of the node current waves shown by Huxley and Stampfli was 1–3 nA; Tasaki (1964) found amplitudes of 4–6 nA. All results from frog are for large (about 14 μm) fibers. For mammals, Maruhashi and Wright (1967) have published a single measurement made in passing of the node current of a "large" sciatic nerve fiber in the rat. They found an amplitude of 6.4 nA. We find that our cat

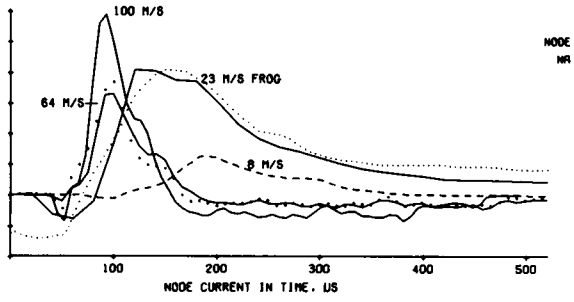

FIGURE 3

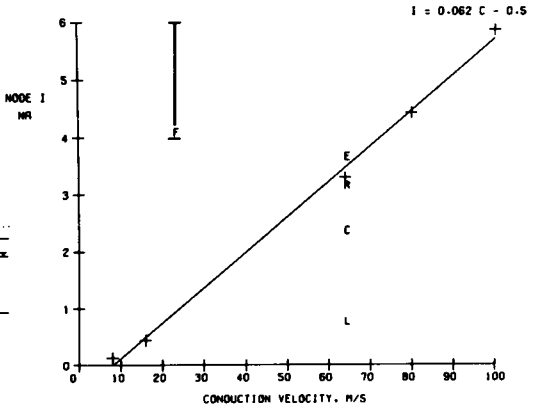

FIGURE 4

FIGURE 3 Node current waveforms calculated from the intra-axonal potential profiles using Eq. 4. The waveform in large dots was calculated from the 64 m/s node potential which was augmented with its time derivative (Fig. 1). The waveform in small dots is the amphibian node current measured by Huxley and Stampfli (1949). The 8 m/s waveform has been multiplied by a factor of 10 for clarity.

FIGURE 4 Node current amplitudes for several mammalian fiber sizes fitted by least squares to a straight line. Letters denote currents for the fibers having modified parameters listed in Table I. *F* is the calculated current of the frog node, bracketed by the range of published measurements.

fibers with diameters in the size range which is large for the rat (10–14 μm) have current amplitudes of 3.3–4.4 nA (Table I).

Fig. 4 shows the amplitude of the node current of five mammalian fibers plotted against their conduction velocity. The fit to a proportional relation is good, and better with a small offset. The lettered point *F* indicates the frog node current, and is bracketed with the range of measured values. For the 64 m/s fiber, *E* indicates the current after the node voltage waveform is modified by adding to it its time derivative times 16.6 μs; *C* shows the effect of reducing the myelin capacity by 40%, and *R*, of increasing value of r_m 10-fold. As discussed above, these changes were suggested by the degree of uncertainty of the data from which they were taken.

EXTRACELLULAR POTENTIALS

Theory

Since the extracellular current densities have transverse and longitudinal components (call them J_x and J_t), the extracellular voltage w within the nerve trunk (and within the space between the nerve trunk and tube wall) has transverse as well as longitudinal gradients. Let us ignore the transverse gradients for the present and work with the weighted average of w over the cross section of the tube. Let $v(x)$ be the average at the section x. In the following derivation we show that $v(x)$ is determined by the total longitudinal extracellular current I_e, and that I_e is determined by $V(x)$, the intra-axonal potential, so that $V(x)$ determines $v(x)$. The derivation is modified from Stein and Pearson (1971). For a rigorous treatment of the currents and fields around nerve fibers, see Clark and Plonsey (1966; 1968) and Plonsey (1974).

Let w be a function of r and θ, the radial and angular coordinates about the center of the tube, so that the nerve trunk can lie eccentrically within the tube: $w = w(r, \theta, x)$. Then s_x, the longitudinal conductivity of the nerve tissue or the space between nerve and tube, will also be a function of r and θ. All integrals are over the cross section of the tube, excluding the fiber under study. Then

$$I_e = \int J_x r \, dr \, d\theta = -\int s_x (\delta w/\delta x) r \, dr \, d\theta$$
$$= -(\delta/\delta x) \int s_x w r \, dr \, d\theta. \tag{8}$$

Now define $v(x)$ and R_e.

$$v(x) = \int s_x w r \, dr \, d\theta / \int s_x \, dr \, d\theta, \tag{9}$$

$$R_e^{-1} = \int s_x r \, dr \, d\theta. \tag{10}$$

Thus $v(x)$ is the average of the potential over the section x, weighted by $s_x(r, \theta)$, and R_e is the longitudinal resistance per length within the tube outside the fiber. Then from Eq. 8

$$I_e = -(1/R_e) \delta v/\delta x. \tag{11}$$

The longitudinal gradients of the intra- and extracellular currents are equal and

opposite:

$$\delta I_e/\delta x = -\delta I_i/\delta x = i, \tag{12}$$

(i is outward myelin current) and the intra-axonal current is proportional to its potential gradient:

$$I_i = -(1/R_i)\delta V/\delta x, \tag{13}$$

where R_i from Eq. 7 is the intra-axonal resistance per length. From Eqs. 11, 12, and 13,

$$\delta^2 v/\delta x^2 = -(R_e/R_i)\delta^2 V/\delta x^2. \tag{14}$$

Assume that $v(x)$ is held at ground potential at the tube ends:

$$v(0) = v(L') = 0. \tag{15}$$

Integrating Eq. 14 twice and then evaluating the two constants of integration using Eq. 15 as boundary conditions, we find

$$v(x) = -(R_e/R_i)[V(x) - (1 - x/L')V(0) - (x/L')(V(L')]. \tag{16}$$

Thus this relation, which was derived by Stein and Pearson (1971) for an unmyelinated fiber in a tube, applies as well to a myelinated fiber in an anisotropic nerve eccentrically placed within a tube, if $v(x)$ is interpreted as the weighted mean potential at x. (All functions of r and θ must be independent of x.) Although departures of the actual potential from $v(x)$ within the section at x will have 0 mean, they will only vanish in the absence of transverse currents. Potentials arising from transverse currents will be treated briefly in a later section.

(Graphically Eq. 16 is obtained by placing a cord, of horizontal extent equal to a tube length, on the graph of $V(x)$ and subtracting this straight line from the contained portion of the waveform. This "cord potential" is then multiplied by $-R_e/R_i$.)

RESULTS

Fig. 5 shows $v(x = L'/2)$, the average extracellular potential at midtube, divided by the factor (R_e/R_i), versus time, for tubes of various lengths, and for various displacements of the central node from midtube for the 64 m/s fiber. These curves were calculated using Eq. 16. The node displacements are given as percentages of the length L of the internode; positive displacements are in the conduction direction. Tube lengths are also given in units of L in the left margin. For a tube of length $L/2$ (top line), a 0% displacement gives a waveform similar to the node current. An effect of the internodal dips is seen for the 50% displacements for tube length $L/2$ and L: the recorded voltage would be identically 0 in the absence of the dips, since no nodes would be within the tube. These voltage waveforms resemble those of the myelin current; the differences in amplitude are related to the resistance associated with tube length.

The signals from tubes of length $1.5L$ and greater are biphasic. For the shorter of

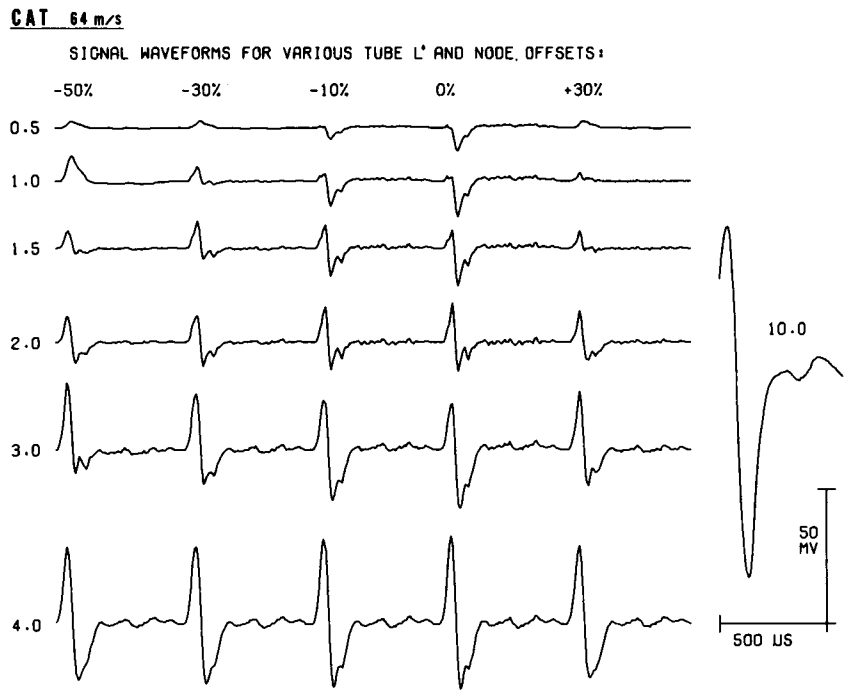

FIGURE 5 Extracellular potential waveform (average across tube) at the midpoint of tubes of various lengths (L'), divided by (R_e/R_i) (Eq. 16). Tube lengths in units of internodal length (L) are given in the left margin, and the displacements of the central node, as percent of L, are shown at the top of each column.

these tubes, the longitudinal position of the nodes and dips affects the waveform of the potential at midtube. For the longer tubes, the waveform is no longer affected by the longitudinal position of the internodal dips, and the temporal phases of the wave occur as the overall spatial profile of the intracellular potential within the tube has a positive, then negative, then positive, curvature. The notch in the trailing edge of the negative phase is a reflection of a reduction in curvature in the empirical node potential ("cat" in Fig. 1) just before its peak, which induces a notch in its second derivative, and is probably caused by noise.

Fig. 6 shows the amplitude of these potentials, divided by R_e, for centrally placed nodes (solid lines) and the range of amplitudes for other placements (vertical bars), plotted against tube length. The course of the central line is disturbed when nodes fall at both the center and both ends (lengths $2L$, $4L$, etc.), but is essentially linear for short lengths. In Fig. 7 the log of v/R_e is plotted against length on a log axis, for tubes up to a wavelength long. For tubes shorter than an internode (see Table I for values of L) the maximum amplitude (centrally placed node) is proportional to tube length. There is a dip at $2L$, and, for lengths longer than the wavelength, an approach to the value 130 mV/R_i (115 mV/R_i for frog) (Stein and Pearson, 1971). The recorded amplitudes, as indicated by Eq. 16, are obtained by multiplying the ordinate of Fig. 6 or 7 by

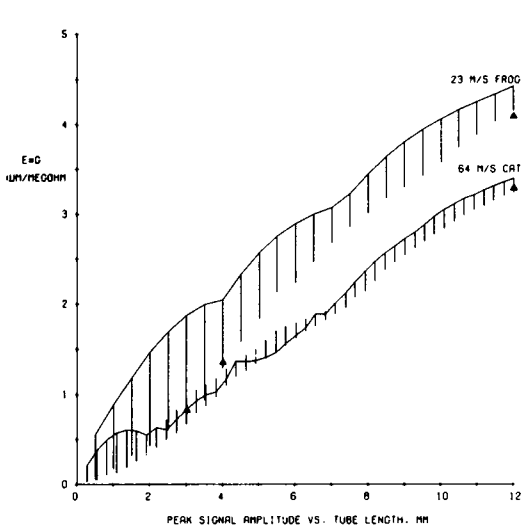

FIGURE 6

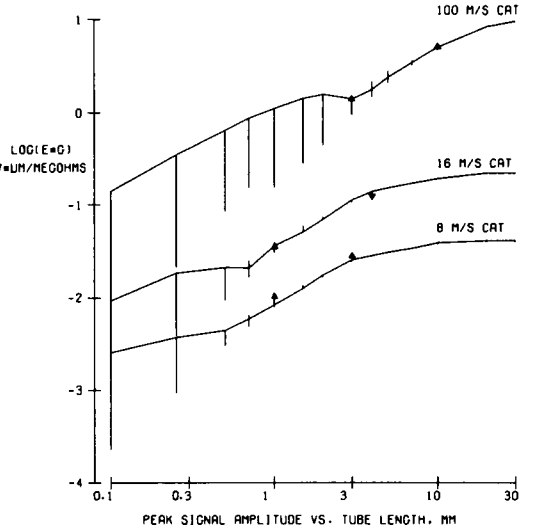

FIGURE 7

FIGURE 6 Extracellular potential amplitudes at midtube, divided by tube resistance per unit length, plotted against tube length. The line shows the potential when a node is at midtube; the bars show the excursions of this for other positions of the central node. The triangles are calculated from the relation $v/R_e = i_{node}/12$, i.e., $v = i_{node} R_t/3$, where R_t is tube resistance.

FIGURE 7 Extracellular potentials as in Fig. 6 for other fibers, plotted as log vs. log. Triangles as described under Fig. 6.

$R_e = K_x/(\pi D^2/4)$, where D is tube diameter, and K_x is typically 2.5 times the resistivity of saline (Tasaki, 1964).

In Figs. 6 and 7, which plot v/R_e vs. L', notice that a portion of each curve to the right of the notch at $L' = 2L$ is straight and proportional to L'. Furthermore, the height of the curves in this range is proportional to i_{node} for each fiber type; the triangles in these figures lie on the lines $v/R_e = i_{node}\ L'/12$. The fit appears to be useful for the larger mammalian fibers. Since the tube resistance, center to ends, is given by $R_t = L'\ R_e/4$, one can summarize the curves for the larger mammalian fibers in this range of tube lengths, $2L < L' < 8L$, with the approximation $v(L'/2) = i_{node} R_t/3$.

The Transverse Currents

Within the nerve trunk, the voltages generated by the transverse component of the current from a fiber are augmented by the transverse resistivity, which Tasaki (1964) finds to be approximately 50 times greater than the longitudinal resistivity ($K_t/K_x = 50$). Plonsey (1974) derives equations for the fields around fibers in anisotropic media. From them one concludes that the equipotential surfaces around a point source within a nerve trunk of infinite diameter are ellipsoids of revolution whose longitudinal axes are the square root of (K_t/K_x) times as long as the radial axes, and that the potential at the coordinates r^*, x from such a source would be

$$u(r^*, x) = (K_t/4\pi)I_{node}/(x^2 + (K_t/K_x)r^{*2})^{1/2}. \quad (17)$$

For the 64 m/s fiber we find a node current amplitude of 3.3 nA, most of which reenters the fiber through the myelin within one internodal distance of the node. Let us neglect this reentry locally, and assume that within 100 μm longitudinally of the node, the current pattern is that of a point sink with source at infinity. Then Eq. 17 predicts, using $K_t/K_x = 50$, that at a radial distance of 30 μm from the fiber, $u(30.0) = 98\,\mu$V.

The voltage induced by the longitudinal current can be read from Fig. 6. Within a 4 mm long tube of diameter $D = 200\ \mu$m, the figure predicts for the voltage at the midpoint

$$v = 1\,(\text{V-}\mu\text{m/M}\Omega)(K_x/(\pi D^2/4) = 52\,\mu\text{V} \quad (18)$$

and for a 1 mm long, 100 μm diameter tube, $v(x = L'/2) = 114\,\mu$V.

Eq. 17 is only approximate, since it omits the myelin currents, the current return at adjacent nodes, and the boundary condition at the walls of the tube. In cross sections of a nerve in this size range for x near a node, the extracellular potential $w(r, \theta, x)$ will be obtained by adding to its average value $v(x)$ a curve $u(r^*, x) - a(x)$, where $u(r^*, x)$ resembles Eq. 17 and has magnitude grossly comparable to $v(x)$, and $a(x)$ biases $u(r^*, x)$ to have zero mean across the tube. Thus $u(r^*, x) - a(x)$ would augment the magnitude of $v(x)$ near the node, and reduce it slightly at larger radial distances. Since u and v are comparable in amplitude we conclude that the potential at the surface of the nerve due to fibers near the surface should be grossly the order of twice that of fibers near the center for tubes in this size range.

Since the local potentials induced by node currents depend strongly on radial distance, their amplitude at the recording contact should be strongly affected by the amount of space outside the nerve and by the proximity of the nerve to the recording contact. The estimates of the longitudinal potentials are unaffected by this space, except through its affect on R_e and the tube resistance, center-to-ends. Although local potentials may be more susceptible to the space outside the nerve trunk, as tube length diminishes or tube diameter increases, the longitudinal potential $v(x)$ decreases and the local potentials from transverse currents may come to dominate a nearby contact.

In Eq. 1, the extracellular voltages were ignored by comparison to the intracellular. The maximum extracellular voltage just outside a node is $u(d/2, 0)$ from Eq. 17. For the 64 m/s fiber this equals 0.83 mV, in comparison with the intracellular amplitude of 130 mV. The total extracellular node-to-node voltage drop is about $2u(d/2, 0)$, since the drop occurs largely near the nodes. Therefore the ratio of node-to-node resistance of the extracellular to the intracellular pathway is this quantity divided by $(i_{node} L\ R_i)$, which is $(K_t/K_i)(K_x/K_t)^{1/2}(d/8L) < 0.02$ for the mammalian fibers.

CONCLUSIONS

The relation between node current and conduction velocity of Fig. 4, combined with the approximate relation $v(L'/2) = \frac{1}{3}I_{node}\ R_t$ obtained from Figs. 6 and 7, gives a simple approximation for the midtube potential in terms of the conduction velocity and

the tube resistance (center to ends). The recorded potential should vary as discussed above depending on the radial position of the fiber and of the nerve bundle, and should vary with longitudinal node position as shown in Figs. 6 and 7.

Although the details of the current and voltage waveforms are subject to revision because only one waveform was available for the mammalian node potential, the magnitudes of these potentials are determined largely by the amplitude and rise-times of these potentials, which are relatively secure. The mammalian myelin resistance may differ considerably from the amphibian value adopted here, but it is probably so great that uncertainties in it have little effect (see Table I). The most serious uncertainty appears to be in the myelin capacitance; the known degree of uncertainty in the amphibian data causes a 40% variation in our predicted node currents.

The graphs were composed using the computer language MLAB written by G. D. Knott.

This work was supported in part by National Institutes of Health Grant NS-08385 and by the Department of Biophysics, The Johns Hopkins University.

Received for publication 31 July 1975 and in revised form 29 December 1975.

REFERENCES

BRINDLEY, G. S. 1972. Electrode arrays for making long-lasting electrical connection to spinal roots. *J. Physiol. (Lond.).* **222**:136P.

CLARK, J., and R. PLONSEY. 1966. A mathematical evaluation of the core conductor model. *Biophys J.* **6**:95.

CLARK, J., and R. PLONSEY. 1968. The extracellular potential field of the single active nerve fiber in a volume conductor. *Biophys. J.* **8**:842.

ECCLES, J. C., and K. KRNJEVIC. 1959. Potential changes recorded inside primary afferent fibers within the spinal cord. *J. Physiol. (Lond.).* **149**:250.

FITZHUGH, R. 1962. Computation of impulse initiation and saltatory conduction in a myelinated fiber. *Biophys. J.* **2**:11.

FRANKENHAEUSER, B., and A. F. HUXLEY. 1964. The action potential in the myelinated nerve fibre of Xenopus Laevis as computed on the basis of voltage clamp data. *J. Physiol. (Lond.).* **171**:302.

GOLDMAN, L., and J. S. ALBUS. 1968. Computation of impulse conduction in myelinated fibers; theoretical basis of the velocity-diameter relation. *Biophys. J.* **8**:596.

HODGKIN, A. L. 1964. The Conduction of the Nervous Impulse. Charles C. Thomas, Springfield, Ill.

HODLER, J., R. STAMPFLI, and I. TASAKI. 1952. Role of potential wave spreading along myelinated nerve in excitation and conduction. *Am J. Physiol.* **170**:375.

HOFFER, J.-A., W. B. MARKS, and W. Z. RYMER. 1974. Nerve fiber activity during normal movements. *Soc. Neurosci. Abstr. No. 300.*

HORAKOVA, M., W. NONNER, and R. STAMPFLI. 1968. Action potentials and voltage clamp currents of single rat Ranvier nodes. *XXIV Int. Congr. Physiol. Soc. No. 594.*

HUXLEY, A. F., and R. STAMPFLI. 1949. Evidence for saltatory conduction in peripheral myelinated nerve fibers. *J. Physiol (Lond.).* **108**:315.

LUBINSKA, L. 1960. Method of isolation of peripheral nerve fibers for quantitative morphological purposes. *Bull. Acad. Pol. Sci. Ser. Sci. Biol.* **8**:117.

MANNARD, A., R. B. STEIN, and D. CHARLES. 1974. Regeneration electrode units: implants for recording from single peripheral nerve fibers in freely moving animals. *Science (Wash. D.C.).* **183**:574.

MARKS, W. B. 1965. Some methods for simultaneous multiunit recording. Proceedings of the Symposium on Information Processing in Sight Sensory Systems, California Institute of Technology, Pasadena, Calif.

MARUHASHI, J., and E. B. WRIGHT. 1967. Effect of oxygen lack on the single mammalian (rat) nerve fiber. *J. Neurophysiol.* **30**:434.

PAINTAL, A. S. 1966. The influence of diameter of medullated nerve fibers of cats on the rising and falling phases of the spike and its recovery. *J. Physiol. (Lond.).* **184**:791.

PAINTAL, A. S. 1967. A comparison of the nerve impulses of the mammalian non-medullated nerve fibers with those of the smallest diameter medulated fibers. *J. Physiol. (Lond.).* **193**:523.

PLONSEY, R. 1974. The active fiber in a volume conductor. *IEEE Trans. Biomed. Eng.* **BME-21**:371.

SANDERS, F. K., and D. WHITTERIDGE. 1946. Conduction velocity and myelin thickness in regenerating nerve fibers. *J. Physiol. (Lond.).* **105**:152.

STAMPFLI, R. 1952. Bau und Funktion isolierter markhaltiger Nervenfasern. *Ergeb. Physiol.* **47**:70.

STEIN, R. B., and K. G. PEARSON. 1971. Predicted amplitude and form of extracellularly recorded action potentials from unmyelinated nerve fibers. *J. Theor. Biol.* **32**:539.

TASAKI, I. 1964. A new measurement of action currents developed by single nodes of Ranvier. *J. Neurophysiol.* **27**:1199.

WILLIAMS, P. L., and C. P. WENDELL-SMITH. 1971. Some additional parametric variations between peripheral nerve fiber populations. *J. Anat.* **109**:505.